

### 20.5 % efficient ternary organic photovoltaics using an asymmetric small-molecular acceptor to manipulate intermolecular packing and reduce

Downloaded from: https://research.chalmers.se, 2025-11-18 14:52 UTC

Citation for the original published paper (version of record):

Ling, Z., Wu, J., Jurado, J. et al (2025). 20.5 % efficient ternary organic photovoltaics using an asymmetric small-molecular acceptor to

manipulate intermolecular packing and reduce energy losses. Materials Science and Engineering: R: Reports, 163. http://dx.doi.org/10.1016/j.mser.2024.100922

N.B. When citing this work, cite the original published paper.

research.chalmers.se offers the possibility of retrieving research publications produced at Chalmers University of Technology. It covers all kind of research output: articles, dissertations, conference papers, reports etc. since 2004. research.chalmers.se is administrated and maintained by Chalmers Library

ELSEVIER

Contents lists available at ScienceDirect

### Materials Science & Engineering R

journal homepage: www.elsevier.com/locate/mser





# 20.5 % efficient ternary organic photovoltaics using an asymmetric small-molecular acceptor to manipulate intermolecular packing and reduce energy losses

Zhaoheng Ling <sup>a,\*,1</sup>, Jingnan Wu <sup>b,c,1</sup>, José P. Jurado <sup>a</sup>, Christopher E. Petoukhoff <sup>a</sup>, Sang Young Jeong <sup>d</sup>, Dipti Naphade <sup>a</sup>, Maxime Babics <sup>a</sup>, Xiaoming Chang <sup>a</sup>, Hendrik Faber <sup>a</sup>, Spyros Doukas <sup>e</sup>, Elefterios Lidorikis <sup>e</sup>, Mohamad Insan Nugraha <sup>a,f</sup>, Mingjie He <sup>a</sup>, Maryam Alqurashi <sup>a</sup>, Yuanbao Lin <sup>g</sup>, Xiaokang Sun <sup>h</sup>, Hanlin Hu <sup>h</sup>, Han Young Woo <sup>d</sup>, Stefaan De Wolf <sup>a</sup>, Leonidas Tsetseris <sup>i</sup>, Frédéric Laquai <sup>a</sup>, Donghong Yu <sup>c,j</sup>, Ergang Wang <sup>b,\*</sup>, Thomas D. Anthopoulos <sup>a,k,\*\*</sup>

- <sup>a</sup> King Abdullah University of Science and Technology (KAUST), KAUST Solar Center (KSC), Thuwal 23955, Saudi Arabia
- <sup>b</sup> Department of Chemistry and Chemical Engineering, Chalmers University of Technology, Göteborg SE-412 96, Sweden
- <sup>c</sup> Department of Chemistry and Bioscience, Aalborg University, Aalborg DK-9220, Denmark
- <sup>d</sup> Department of Chemistry, Korea University, Anam-ro 145, Seoul 02841, Republic of Korea
- <sup>e</sup> Department of Materials Science and Engineering, University of Ioannina, Ioannina 45110, Greece
- <sup>f</sup> Research Center for Nanotechnology Systems, National Research and Innovation Agency (BRIN), South Tangerang, Banten 15314, Indonesia
- g College of Education Sciences, The Hong Kong University of Science and Technology (Guangzhou), Guangzhou 510000, China
- h Hoffmann Institute of Advanced Materials, Shenzhen Polytechnic, 7098 Liuxian Boulevard, Shenzhen 518055, China
- i Department of Physics, School of Applied Mathematical and Physical Sciences, National Technical University of Athens, Athens GR-15780, Greece
- <sup>j</sup> Sino-Danish Center for Education and Research (SDC), Aarhus DK-8000, Denmark
- k Henry Royce Institute, Photon Science Institute, Department of Electrical and Electronic Engineering, The University of Manchester, Oxford Road, Manchester M13 9PL,

#### ARTICLE INFO

## Keywords: Asymmetric non-fullerene small molecular acceptor Energy loss Intermolecular packing

High efficiency ternary organic photovoltaics

#### ABSTRACT

Oligomeric acceptors are increasingly recognized as promising n-type materials for organic photovoltaics (OPVs) due to their precise molecular structures, long-term stability, and high efficiency. However, inferior molecular packing and high energy losses have hindered their further use. Here, we overcome these challenges by developing an asymmetric small molecular acceptor (SMA), BTP-J17, and applying it as the second acceptor component in OPVs composed of PM6:DIBP3F-Se:BTP-J17 (refer to our recent work on dimeric acceptor DIBP3F-Se). The BTP-J17 is very miscible with the DIBP3F-Se and appears to diffuse into the host donor-acceptor interface. The ensuing ternary cells exhibit enhanced exciton dissociation, improved carrier mobility, and more efficient charge extraction. Optimised OPVs based on PM6:DIBP3F-Se:BTP-J17 show enhanced open-circuit voltage ( $V_{\rm OC}$ ) while maintaining the high short-circuit current ( $J_{\rm SC}$ ) from the binary blends, boosting the power conversion efficiency (PCE) from 18.40 % to 19.60 %. By integrating MgF<sub>2</sub> as an antireflection coating and n-doping the ternary BHJ with ethyl viologen (EV), we were able to further boost the PCE to 20.5 % (uncertified) and simultaneously extended the outdoor stability to seven weeks. Our findings highlight the crucial role of asymmetric SMA as an additional component for boosting the performance and stability of OPVs.

<sup>\*</sup> Corresponding authors.

<sup>\*\*</sup> Corresponding author at: Henry Royce Institute, Photon Science Institute, Department of Electrical and Electronic Engineering, The University of Manchester, Oxford Road, Manchester M13 9PL, UK.

E-mail addresses: zhaoheng.ling@kaust.edu.sa (Z. Ling), ergang@chalmers.se (E. Wang), thomas.anthopoulos@manchester.ac.uk (T.D. Anthopoulos).

<sup>&</sup>lt;sup>1</sup> These authors contributed equally,

#### 1. Introduction

Organic photovoltaics (OPVs) are rapidly emerging as a promising renewable energy source, characterized by numerous attractive attributes, including promising power conversion efficiency (PCE), tunable optical transparency and potential for low-cost manufacturing via solution processing techniques [1–9]. In recent years, significant advancements have been made in enhancing the performance of small molecular acceptor (SMA) OPVs, achieving PCEs over 20 % through the synthesis of new organic molecules with varied functionalities, optimization of film morphology, utilization of innovative charge-transporting layers and engineering of device architectures [10–19]. However, high-performance SMA-OPVs often lack long-term stability and mechanical robustness, primarily due to blend morphology degradation caused by rapid SMA molecule diffusion under light irradiation and heat, which stems from their low glass-transition temperatures ( $T_g$ ) and high diffusion coefficients [20–22].

To overcome these challenges, oligomeric acceptors (OAs) such as dimeric molecules have recently been developed, enabling OPVs that combine high PCE with enhanced stability [18,23]. For example, Lee et al., reported OPV based on DYBO (a dimerized YBO (butyloctyl-Y6) molecule) linked with a benzodithiophene unit, achieving a PCE of 18.1 % and operational stability ( $T_{80}$ ) exceeding 6000 hours [24]. Deng et.al reported dimer-2CF-based OPVs with efficiency of 19.02 % and a fill factor (FF) of > 80 % and an extrapolated  $T_{80}$  of approximately 12, 000 h under continuous heating at 80 °C [25]. Despite these advantages, the extended conjugated structures in OAs can produce various molecular conformations due to the rotatable C-C single bonds between the conjugated moieties (SMA segments) and linkers, leading to a twisted backbone with dihedral angles greater than 20°, which adversely affects molecular packing, blend morphology and ultimately charge carrier transport [26,27]. In our previous study, we synthesized a dimerized acceptor, DIBP3F-Se, by linking a Y6 derivative with a selenophene bridge unit and adopting an O-shaped conformation, facilitated by a unique 'conformational lock' from robust intramolecular  $\pi$ - $\pi$  interactions between the terminal IC groups, achieving a PCE exceeding 18 % [28]. Nonetheless, the relatively low molecular packing of these dimers resulted in a higher recombination rate than those in SMA-based OPVs. It has been reported that asymmetric non-fullerene acceptors with larger dipole moments can enhance molecular packing, yield a noticeable blue-shift in light absorption, and reduce voltage loss when being incorporated as the third component [29–31].

Here, we synthesized an asymmetric non-fullerene SMA BTP-J17 and incorporated it as a third component into the PM6:DIBP3F-Se blend. The BTP-J17 was found to diffuse into the host donor/acceptor interface, resulting in enhanced charge separation and higher charge carrier mobilities. Crucially, BTP-J17 reduced energy loss by facilitating a homogenous distribution of DIBP3F-Se and enhancing molecular packing, thereby improving the open-circuit voltage ( $V_{\rm OC}=0.941$  V) while maintaining a high  $J_{\rm SC}$  (26.7 mA cm $^{-2}$ ) leading to OPVs with a maximum PCE of 19.6 %. N-doping the ternary PM6:DIBP3F-Se:BTP-J17 (1:1:0.6 (wt%)) blend with ethyl viologen (EV) and using MgF $_2$  as an antireflection coating boost the PCE to a maximum value of 20.5 % (uncertified). The ensuing ternary-based OPVs exhibit enhanced operating stability and can maintain 80 % of their initial PCE after 7 weeks of continuous outdoor testing in a hot and humid environment in Saudi Arabia.

#### 2. Results and discussion

To enhance the absorption spectrum of PM6:DIBP3F-Se, we designed and synthesized the small molecular acceptor BTP-J17 (Fig. 1a). The synthetic procedures and molecular structure characterizations of BTP-J17 are detailed in Scheme S1 and Figures S2, S3 in the experimental session of supporting information (SI). The ultraviolet-visible near-infrared (UV-vis-NIR) light absorption spectra of PM6, DIBP3F-Se, and

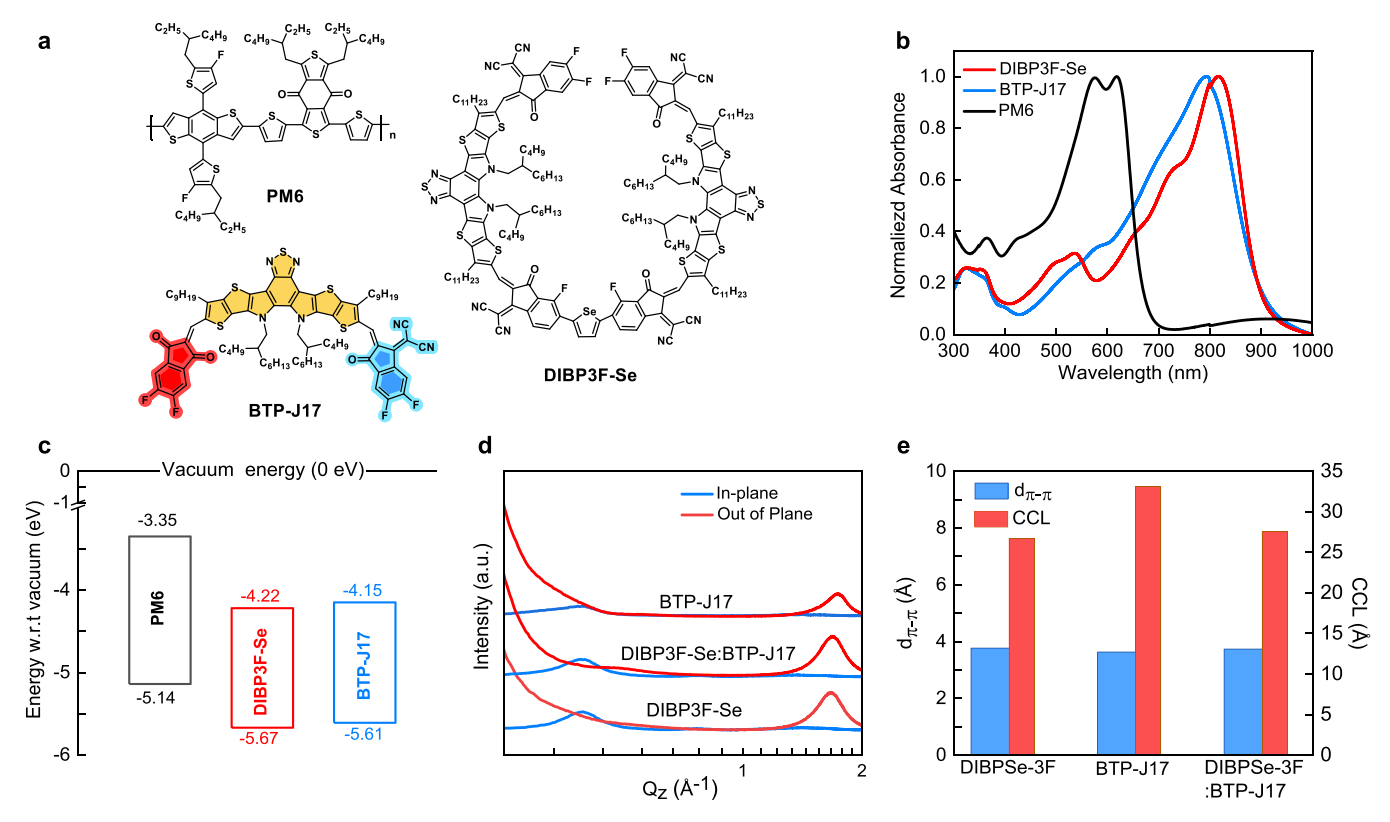


**Fig. 1.** Structure and physical properties of the active materials used in this study. (a) Molecular structures of PM6, DIBP3F-Se, and BTP-J17. (b) The absorption spectra of the PM6, DIBP3F-Se, and BTP-J17 neat films. (c) Energy levels of PM6, DIBP3F-Se, and BTP-J17. (d) The corresponding IP and OOP profiles of DIBP3F-Se and BTP-J17 acceptor films. (e) The CCL and  $d_{\pi_{\pi}\pi}$  values of the DIBP3F-Se and BTP-J17 acceptor films.

BTP-J17 were presented in Fig. 1b. The absorption peaks for PM6, DIBP3F-Se, and BTP-J17 are located at 620 nm, 825 nm, and 800 nm, respectively, indicating complementary absorptions that enhance the light-harvesting capabilities of the ternary blend from visible to near-infrared light spectrum range. The highest occupied molecular orbital (HOMO) levels of the donor and acceptor were measured using photo-electron spectroscopy in air (PESA), and the lowest unoccupied molecular orbital (LUMO) levels were calculated by adding the optical band gap to their respective HOMO levels (Fig. 1c and Figure S4). The LUMO and HOMO levels of DIBP3F-Se and BTP-J17 were determined to be  $-4.22 \, \mathrm{eV}$ ,  $-5.67 \, \mathrm{eV}$ , and  $-4.15 \, \mathrm{eV}$ ,  $-5.61 \, \mathrm{eV}$ , respectively. Notably, the LUMO and HOMO levels of BTP-J17 exhibit a slight upshift relative to those of DIBP3F-Se. The narrow HOMO offset between PM6 and BTP-J17 is expected to reduce non-radiative voltage losses [32].

Grazing incidence wide angle X-ray scattering (GIWAXS) was used to examine the molecular packing of the neat films (Fig. 1d, S5 and Table S1). In GIWAXS measurements, d-spacing refers to the distance between planes in a crystal lattice. A smaller d-spacing means the crystal planes are closer together, which indicates that the molecules are more tightly packed. The crystal coherence length (CCL) refers to the average size of ordered regions or domains within the material, with a larger CCL indicating the presence of more well-ordered regions/domains. In the inplane (IP) direction, peaks observed at  $\sim$ 0.39 Å<sup>-1</sup> for both DIBP3F-Se and BTP-J17 films indicate a face-on molecular orientation. The (010) diffraction peak is located at  $q_z$ = 1.667  $\mathring{A}^{-1}$  for DIBP3F-Se and  $1.730~\mbox{Å}^{-1}$  for BTP-J17 films in the out-of-plane (OOP) direction, corresponding to the d-spacing for  $\pi$ - $\pi$  stacking of 3.77 Å and 3.63 Å, respectively. Furthermore, the CCL was quantified as 26.74 Å and 33.07 Å for DIBP3F-Se and BTP-J17 neat films, respectively, using the Scherrer equation [33]. These results suggest that BTP-J17 exhibits stronger self-organization and crystalline order than DIBP3F-Se. The DIBP3F-Se:BTP-J17 blend film, containing 60 wt% (refer to donor weight) BTP-J17, shows more ordered face-on packing, with a  $\pi$ - $\pi$ stacking distance of 3.74 Å and a corresponding CCL of 27.56 Å in the OOP direction. The thermal stability of BTP-J17 was also assessed by thermogravimetric analysis (TGA), as shown in Figure S6a, revealing good thermal stability with a decomposition temperature (5 % weight loss) of approximately 325 °C in nitrogen. The UV-vis deviation metric result for BTP-J17 was also extracted and shown in Figure S6c. The data reveals a lower Tg of ~83 °C compared with DIBP3F-Se.

The miscibility between DIBP3F-Se and BTP-J17 was assessed through contact angle measurements using solvents with different polarities (Figure S7). Subsequently, the surface energies of the distinct layers were determined using the Owens, Wendt, Rabel, and Kaelble (OWRK) method (Table S2). The PM6, DIBP3F-Se, and BTP-J17 solid films exhibit surface energies of 20.49, 25.66, and 22.05 mN/m<sup>2</sup>, respectively. Then, miscibility was evaluated using the Flory-Huggins interaction parameter ( $\chi$ ) [34], where a smaller value indicates a better miscibility. The χ value between the donor PM6 and SMA DIBP3F-Se  $(\chi^{D-A})$  was 0.290, but only 0.028 between PM6 and BTP-J17. After adding 60 wt% BTP-J17 to the DIBP3F-Se film, the  $\chi^{D-A}$  was found significantly decreased to 0.064, suggesting that DIBP3F-Se and BTP-J17 could form a well-mixed acceptor phase in the ternary blend. It has been reported that improved miscibility between acceptors enhances the crystallization of both the donor and acceptor [35]. The presence of the third component at the donor/acceptor interface reduces trap-assisted recombination losses while enhancing exciton dissociation and overall charge transport. These synergistic improvements led to significantly higher FF and short-circuit current ( $J_{SC}$ ) in the device. To examine this possibility, we calculated the interfacial tension between DIBP3F-Se and BTP-J17 using Wu's equation [36]:

$$\gamma_{A-B} = \gamma_A + \gamma_B - 4\left(\frac{\gamma_A^d \gamma_B^d}{\gamma_A^d + \gamma_B^d} + \frac{\gamma_A^p \gamma_B^p}{\gamma_A^p + \gamma_B^p}\right) \tag{1}$$

Here,  $\gamma_{A-B}$  is the interfacial tension between the compound A and B,

while  $\gamma_A^d$  and  $\gamma_A^p$  are the dispersion and polar components of  $\gamma_A$ . The calculated results are summarized in Table S3. The interfacial tension values  $\gamma_{PM6-DIBP3F-Se}$ ,  $\gamma_{PM6-BTP-J17}$ ,  $\gamma_{PM6-DIBP3F-Se:BTP-J17}$  derived were 0.603, 0.103, 0.332 mN m<sup>-1</sup>, respectively, indicating that BTP-J17 can tune the miscibility between PM6 and DIBP3F-Se. To identify where BTP-J17 is located in the ternary blend layer, the wetting coefficient ( $\omega$ ) of the third component is introduced, which is calculated by the Young's equation [37]:

$$\omega_{A_2} = \frac{\gamma_{A_1/A_2} - \gamma_{D/A_2}}{\gamma_{D/A_1}} \tag{2}$$

Here,  $\gamma_{A_1/A_2}$ ,  $\gamma_{D/A_2}$ ,  $\gamma_{D/A_1}$  correspond to  $\gamma_{DIBP3F-Se/BTP-J17}$ ,  $\gamma_{PM6/BTP-J17}$  and  $\gamma_{PM6/DIBP3F-Se}$ , respectively. It has been reported that component  $A_2$  resides in the phase of component D when the wetting coefficient exceeds 1 and in the domain of component  $A_1$  if  $\omega_{A2} < -1$ . If  $-1 < \omega_{A2} < 1$ , then component  $A_2$  is situated at the interfaces between D and  $A_1$ . In our case,  $\omega_{BTP-J17}$  was calculated to be 0.441, suggesting that BTP-J17 is located, primarily, at the PM6/DIBP3F-Se interface. We hypothesize that this interfacial localization of BTP-J17 within the donor/acceptor blend creates additional charge transport pathways, thereby enhancing exciton separation and carrier transport [35].

To evaluate the influence of BTP-J17 on the host PM6:DIBP3F-Se blend, OPVs were fabricated with a conventional structure comprising ITO/Br-2PACz/Active Layer/PNDIT-F3N/Ag (Fig. 2a). Details of the device preparation process can be found in the SI. Fig. 2b displays the current density versus voltage (J–V) characteristics for the optimal binary and ternary devices, with the corresponding photovoltaic parameters summarized in Table 1. The binary PM6:DIBP3F-Se OPVs exhibit a PCE of 18.40 %, with a  $V_{\rm oc}$  of 0.922 V, a  $J_{\rm sc}$  of 26.13 mA cm<sup>-2</sup>, and an FF of 76.39 %. Cells based on the binary PM6:BTP-J17 BHJ yield a lower PCE of 17.12 %, a high  $V_{\rm oc}$  of 0.965 V, a  $J_{\rm sc}$  of 24.20 mA cm<sup>-2</sup>, and an FF of 73.67 %. The higher voltage in the latter is attributed to the higher LUMO of BTP-J17, highlighting the potential to enhance the voltage of ternary OPVs by incorporating BTP-J17 as the third component.

To test this hypothesis, BTP-J17 was added into the PM6:DIBP3F-Se blend formulation to form the ternary blends. As the weight ratio (wt%) of BTP-J17 increased, a gradual increase in  $V_{\rm oc}$  was observed (Table S4). For a 60 wt% BTP-J17 ratio, the PM6:DIBP3F-Se:BTP-J17 OPV achieves an optimal PCE of 19.60 %, delivering a  $V_{\rm oc}$  of 0.941 V, a  $J_{\rm sc}$  of 26.70 mA cm $^{-2}$  and a FF of 78.01 %. Compared with the binary PM6: DIBP3F-Se system, the improvement in these three crucial OPV parameters demonstrates the successful incorporation of BTP-J17 as the third component, boosting the OPV performance as intended. To verify the reliability of the efficiency value obtained, 20 individual binary and ternary BHJ-based OPVs were fabricated, with the obtained results summarized in Figure S8. The efficiencies of PM6:DIBP3F-Se and PM6: DIBP3F-Se:BTP-J17 devices lie at 18.2 % and 19.3 %, respectively. All three parameters exhibit a narrow distribution, indicating high reproducibility of the OPVs.

The external quantum efficiency (EQE) spectra of the optimal binary and ternary devices is presented in Fig. 2c. Notably, the ternary device exhibits a higher photo-response between 475 and 820 nm than the binary ones based on PM6:DIBP3F-Se, consistent with the higher absorption coefficient of BHJ films, as displayed in Figure S9, indicating that more incident photons are converted to external photocurrent. The integrated photocurrent ( $J_{cal}$ ) was 25.58 and 26.10 mA cm<sup>-2</sup> for the binary and ternary BHJ OPV in good agreement (within 3 %) with the  $J_{SC}$  measured under simulated solar illumination. Additionally, the EQE response of the ternary device reaches 80 % in the range of 500–800 nm, contributing to the enhanced  $J_{sc}$  (by ~2.1 %), as shown in Table 1.

Efforts to increase the PCE of our best-performing OPVs were further performed by using an antireflection coating while simultaneously implementing n-doping of BHJ with the recently developed molecular dopant EV. The experimental details about the preparation of the EV solution and its addition to the BHJ are given in the Supporting

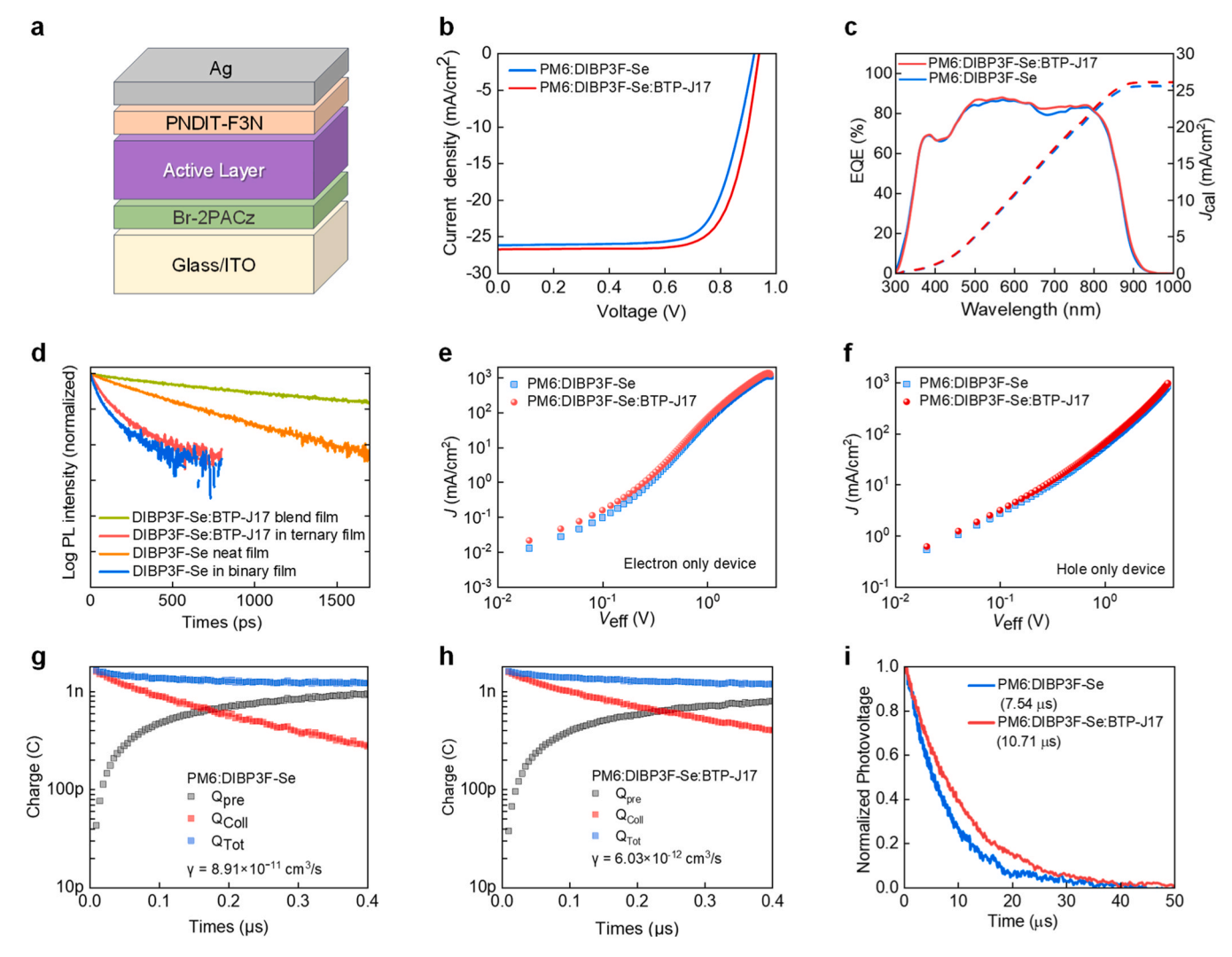


Fig. 2. Solar cell architecture and characterization. (a) Schematic structure of the cells developed in this study. (b) J-V characteristics of the different cells. (c) EQE spectra obtained from the corresponding OPVs. (d) TRPL decays of binary and ternary BHJ systems; J-V curves measured for electron-only (e) and hole-only (f) devices based on the binary and ternary BHJs. (g) TDCF measurements of PM6:DIBP3F-Se and PM6:DIBP3F-Se OPVs. (h) TDCF measurements of PM6:DIBP3F-Se and PM6:DIBP3F-Se:BTP-J17 OPVs.

**Table 1**Summary of photovoltaic parameters of cells based on PM6:BTP-J17, PM6: DIBP3F-Se, and PM6:DIBP3F-Se:BTP-J17, measured under 1-sun illumination.

| внј                       | $J_{\rm sc}$ (mA/ cm <sup>2</sup> ) | $J_{\rm cal}$ (mA/ cm <sup>2</sup> ) <sup>a</sup> | <i>V</i> <sub>oc</sub> (V)    | FF<br>(%)                  | PCE<br>(%) <sup>b</sup>      |
|---------------------------|-------------------------------------|---------------------------------------------------|-------------------------------|----------------------------|------------------------------|
| PM6:BTP-J17               | 24.20<br>(24.07<br>± 0.18)          | 23.30                                             | 0.965<br>(0.963<br>± 0.002)   | 73.67<br>(73.21<br>± 0.33) | 17.12<br>(17.06<br>± 0.09)   |
| PM6:DIBP3F-<br>Se         | $26.13$ $(26.01$ $\pm 0.11)$        | 25.58                                             | $0.922$ $(0.920$ $\pm 0.003)$ | 76.39<br>(75.88<br>± 0.21) | $18.40$ $(18.14$ $\pm 0.13)$ |
| PM6:DIBP3F-<br>Se:BTP-J17 | $26.70 \\ (26.47 \\ \pm 0.12)$      | 26.10                                             | $0.941$ $(0.938$ $\pm 0.002)$ | 78.01 (77.45 $\pm$ 0.26)   | $19.60$ $(19.28$ $\pm 0.14)$ |

<sup>&</sup>lt;sup>a</sup> The current density of champion device calculated from EQE spectra.

Information. As an antireflection layer, we employed a MgF $_2$  due to its low refractive index, lowering the reflection and thus increasing light transmission through the glass substrates [38]. On the other hand, EV was chosen due to its ability to enhance the  $\pi-\pi$  stacking and increase

the absorption coefficient and overall performance of relevant OPVs [39]. To evaluate the effectiveness of these strategies, we first evaluated the impact of MgF2 thickness on optical transmission (Figure S10a). Using these data, the photocurrent extraction was estimated, allowing for the optimal MgF2 thickness to be determined (approx. 100 nm) (Figure S10b-d). Using these design parameters, the optimal EV concentration was determined (Figure S11 and Table S5). MgF2 increases the light absorbed by the BHJ, an effect that is further enhanced when combined with EV-doped BHJs (Figure S11a,d,g). The EQE data reveals that the introduction of MgF2 and EV increase the cell's photoresponse between 400 and 820 nm (Figure S11c,f,i) with FF and J<sub>sc</sub> undergoing similar improvements. As a result, the optimized cells yield a staggering maximum PCE value (uncertified) of 20.5 % ( $V_{oc} = 0.942 \, V, \, FF =$ 78.35 %, and  $J_{\rm sc}=27.85~{\rm mA~cm^{-2}}$ ). These results underscore the importance for simultaneous improvement of the OPV's photonic structure and BHJ properties.

Steady-state photoluminescence (PL) and time-resolved photoluminescence (TRPL) [40,41] experiments were also conducted to study the exciton and charge carrier dynamics among PM6, DIBP3F-Se and BTP-J17, with data analysis details described in Figure S4, Figures S12-S14 and Fig. 2d. For the neat films, Figure S4 shows that the absorption of DIBP3F-Se and BTP-J17 overlaps spectrally with the

 $<sup>^{\</sup>rm b}$  The average PCE values with standard deviations obtained from 20 independent cells.

emission from PM6, supporting energy transfer from PM6 to DIBP3F-Se and BTP-J17 [42]. TRPL spectra and kinetics for PM6, DIBP3F-Se, and BTP-J17 neat films are presented in Figure S12 and Table S6. Color contour plots of the TRPL data (Figure S12a-c) reveal that the BTP-J17 molecule has a significantly longer lifetime than the DIBP3F-Se acceptor molecule. Neat PM6 shows fluence-independent decays over two orders of magnitude, from 0.17 to 17.3 nJ/cm² (Figure S12d). Both neat acceptors begin to exhibit weak fluence-dependence at approx. 17.3 nJ/cm² (Figure S12e,f). As such, a constant fluence of 1.73 nJ/cm² was used for all films (neat and blend layers). No spectral shifts with increasing fluence are observed (Figure S12e,i) and the neat films exhibited average photoluminescence lifetimes ( $\tau$ ) of 468.6, 275.6, and 1185 ps for PM6, DIBP3F-Se, and BTP-J17, respectively, at low excitation fluence.

To accurately compare the quenching efficiencies between the binary and ternary systems, consideration of the lifetime of the acceptor binary blend (DIBP3F-Se:BTP-J17; Figure S13) is necessary. The TRPL spectra of the binary blend exhibited the same shape and emission peak as those of the neat acceptors (Figure S13a,c). It also showed similar fluence-dependence: none up to a fluence of 17.3 nJ/cm², where it only started to deviate from the lower fluence decays. However, the lifetime of the binary blend is markedly longer than that of neat DIBP3F-Se, approaching that of BTP-J17 (Figure S13d). As such, the lifetime of the binary blend was used for calculating the quenching efficiency for the ternary system. As a result, after blending the two acceptors,  $\tau$  was 877.0 ps, roughly the weighted average of the  $\tau$  of the two neat acceptors (Table S6).

The impact of BTP-J17 within the exciton dynamics in the BHJ active layer was also studied by PL quenching efficiency (PLQE) measurements (Fig. 2d and Figure S14). The PLQE is obtained as (1 -  $\tau_{blend}/\tau_{neat}$ ), where  $\tau_{blend}$  and  $\tau_{neat}$  represent the average lifetimes of the blend and neat materials, respectively. PL was observed from both the acceptors  $\sim$ 870 nm and PM6  $\sim$ 670 nm in the blend systems (Figure S14). For both systems, the PM6 emission was quenched > 99 % (Table S6), such that the decay was instrument response function (IRF)-limited (Figure S14c, f), which is typical for energy transfer from donors to non-fullerene acceptors (NFAs) [42]. PM6 was quenched to a greater degree (99.45 %) in the ternary system compared to the binary system (99.24 %), revealing that the introduction of BTP-J17 can further quench the PL of PM6, indicating more efficient energy transfer from PM6 to the acceptors. For the acceptor emission, the PLOE value increased from 89.19 % for the binary blend to 94.93 % for the ternary blend, suggesting greater charge generation efficiency after the incorporation of BTP-J17 [42].

These results are in line with the increasing  $J_{\text{SC}}$  and changing EQE from devices, indicating the BTP-J17 influences the charge generation within ternary BHJ. This conclusion is also supported by the transient photocurrent (TPC) measurement in Figure S15a. The ternary devices deliver a shorter extraction lifetime (0.2  $\mu$ s) than the binary systems (0.315  $\mu$ s), suggesting more efficient extraction for photogenerated carriers in the ternary devices.

For a more comprehensive understanding of the  $J_{sc}$  improvement, we measured the hole  $(\mu_h)$  and electron mobilities  $(\mu_e)$  utilizing the space-charge limited current (SCLC) technique (Fig. 2e, f and Table S7). The hole and electron mobilities of PM6:DIBP3F-Se devices are  $2.67 \times 10^{-4}$  and  $2.29 \times 10^{-4}$  cm $^2$  V $^{-1}$  s $^{-1}$ , respectively. For the PM6:DIBP3F-Se: BTP-J17, the hole and electron mobilities have increased to  $3.02 \times 10^{-4}$  and  $2.68 \times 10^{-4}$  cm $^2$  V $^{-1}$  s $^{-1}$ . Additionally, the  $\mu_h/\mu_e$  ratio for the PM6:DIBP3F-Se device is 1.164, while a smaller value of 1.125 was achieved for the PM6:DIBP3F-Se device, contributing to the improved  $J_{sc}$  due to better-balanced charge transport. Besides, we investigated the charge transport process via the photo-induced charge carrier extraction technique using a linearly increasing voltage (Photo-CELIV) (Figure S15b and Table S8). The carrier mobility  $(\mu)$  in both systems was determined using  $\mu = 2 d^2/(3At^2_{max}(1+0.36 \Delta j/j_0))$ . Here,

d is the thickness of the active layer,  $t_{\rm max}$  is the time to reach the extraction current maximum, A is the voltage rise speed of the applied voltage pulse,  $\Delta j$  and  $j_0$  is a shifting and initial current step, respectively. The extracted  $\mu$  value for PM6:DIBP3F-Se:BTP-J17 device is  $1.95\times10^{-3}$  cm  $^2~{\rm V}^{-1}~{\rm s}^{-1}$  and higher than that for PM6:DIBP3F-Se device  $(1.77\times10^{-3}~{\rm cm}^2~{\rm V}^{-1}~{\rm s}^{-1})$ , consistent with SCLC measurements. Thus, we infer that the changes in the charge transport following the addition of BTP-J17 into BHJ are key contributing factors for the enhanced  $J_{\rm SC}$  and FF in Table 1.

To elucidate differences in geminate recombination and bimolecular recombination before and after BTP-J17 introduction, we performed time-delayed collection field (TDCF) measurements [43]. The normalized total extracted charge at different pre-bias voltages ( $V_{\text{pre}}$ ), shown in Figure S16a, demonstrates that both devices exhibited field dependent charge generation, which was less pronounced in PM6:DIBP3F-Se: BTP-J17 devices. This reduction in field-dependent charge generation could indicate a reduction in geminate recombination. The latter was further evidenced by the significant lowering of the slope (1.226 k<sub>B</sub>T/q to 1.174  $k_BT/q$ ) in the dependence of  $V_{OC}$  on the light intensity ( $P_{light}$ ) (Figure S16b), which also points to a reduction in geminate recombination. Using variable time delay TDCF measurements, we also investigated the systems' bimolecular recombination coefficient ( $\gamma$ ), which is typically on the order of  $10^{-11}$  cm<sup>3</sup> s<sup>-1</sup> for high-efficiency Y-NFAs [44]. Here, the γ values for PM6:DIBP3F-Se and PM6:DIBP3F-Se:BTP-J17 are  $8.91 \times 10^{-11}$  and  $6.03 \times 10^{-12}$  cm<sup>3</sup> s<sup>-1</sup>, respectively, indicating a reduction in bimolecular recombination after BTP-J17 incorporation (Fig. 2g,h). Similar results were obtained by calculating the bimolecular recombination rate constants ( $k_{rec}$ ) using  $k_{rec} = 1/[(\lambda + 1)]n\tau$  [39]. The incorporation of BTP-J17 as the third component resulted in lower k<sub>rec</sub> values, contributing to the suppression of bimolecular recombination and enhancing the overall performance of OPV cells (Figure S17a, b).

Additionally, we investigated the dynamics of charge recombination in both devices using transient photovoltage (TPV) (Fig. 2i). The charge carrier lifetime ( $\tau$ ) of PM6:DIBP3F-Se:BTP-J17 was found to be longer than that of PM6:DIBP3F-Se devices (10.71  $\mu$ s versus 7.54  $\mu$ s), showing a lower carrier recombination rate. Analysis of the interface and bulk resistances in both types of OPVs, we also carried out using electrochemical impedance spectroscopy (EIS) [45] in the dark with the application of  $V_a = V_{\rm OC}$ . The Nyquist plots measured for these devices are shown in Figure S17c. The PM6:DIBP3F-Se:BTP-J17 OPVs exhibited lower interface (R<sub>int</sub>) and BHJ (R<sub>bhj</sub>) resistances than those of the PM6:DIBP3F-Se OPVs, leading to a higher FF and PCE value.

To gain deeper insights into the origin of the enhanced performance, we examined the nanoscale morphologies and molecular packing of the PM6:DIBP3F-Se and PM6:DIBP3F-Se:BTP-J17 films. Figs. 3a and 3b present the atomic force microscopy (AFM) height and phase images for both binary and ternary films, while the AFM images of the neat films are displayed in Figure S18. Both binary and ternary blend films exhibit similar fibrous surface morphologies, which are conducive to effective charge carrier transport. Furthermore, the films maintain the smoothness with a root-mean-square (RMS) roughness value of 885 pm after including the BTP-J17 (Fig. 3e). The smooth surface is attributed to the good miscibility between DIBP3F-Se and BTP-J17. Kelvin probe force microscopy (KPFM) was used to analyze the surface contact potentials (SCP) of the active layers, providing insights into the variations of the built-in potential (V<sub>bi</sub>) in devices [46]. Fig. 3c,d reveal the resultant SCP maps and Fig. 3f displays the distributions extracted along the lines. Both films exhibit an advantageous homogeneous distribution of contact potentials. Moreover, the ternary blend displays higher overall contact potentials spread across the surfaces, as clearly depicted in Fig. 3f. Specifically, the SCPs are determined to be -0.18 V and -0.15 V for the binary and the ternary film, respectively. The higher surface potentials in the ternary active layer indicate an amplified  $V_{\rm bi}$  and larger driving forces to separate excitons and transport charges, thereby enhancing the  $J_{\rm SC}$  and FF in cells [46]. Therefore, it is evident that the ternary blend forms fibrous-like nanoscale networks while exhibiting more favorable

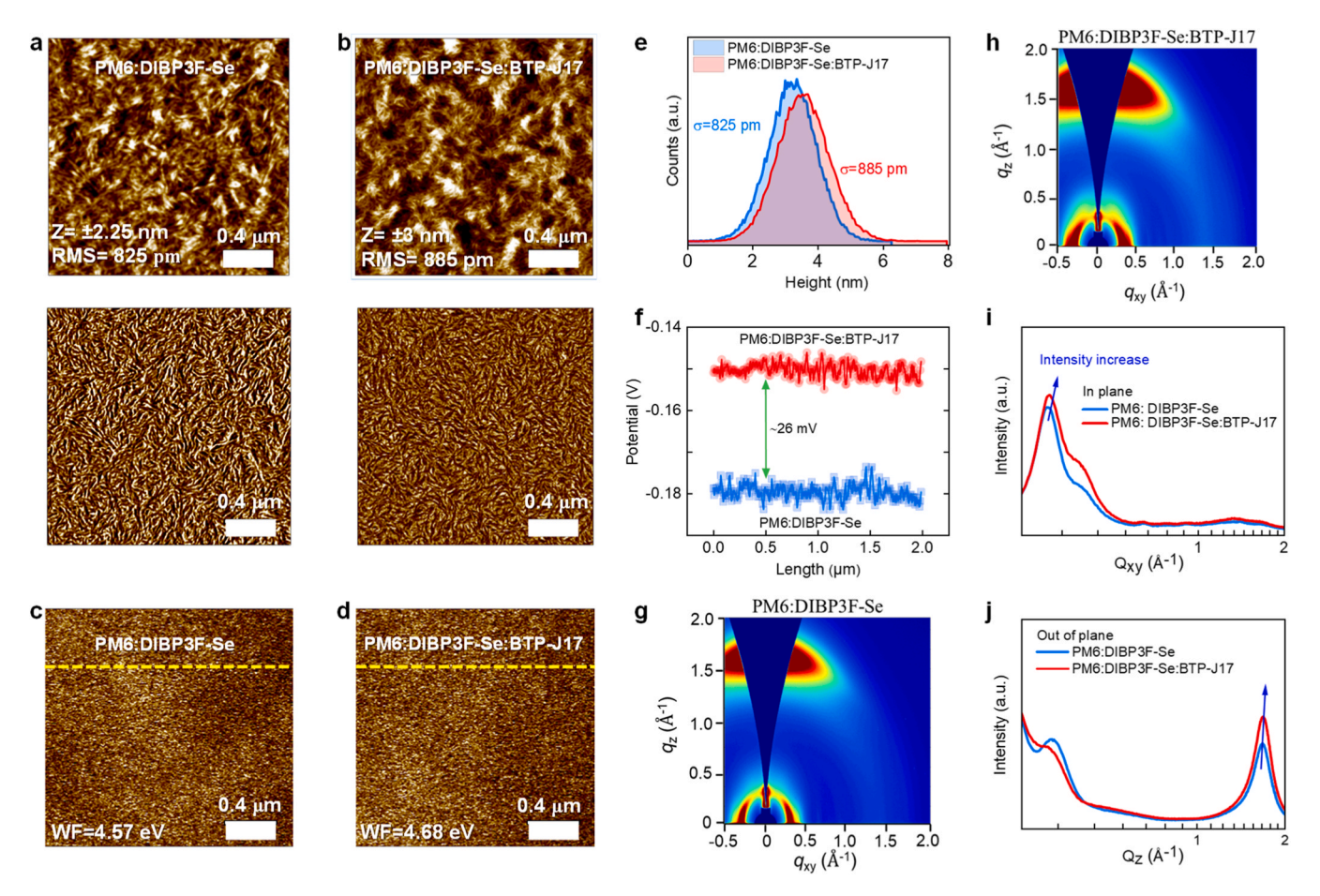


Fig. 3. Morphological characterizations of different blend layers. (a)-(b) Top images: AFM Phase images of the relevant blends. (c)-(d) KPFM images of relevant blends. (e) Surface height distribution of relevant blends. (f) Surface potentials measured for the binary and ternary blends. (g)-(h) 2D GIWAXS patterns of the relevant BHJs. (i)-(j) IP and OOP extracted line-cut profiles for the two blend layers.

surface potentials. As the binary and ternary films exhibit similar RMS values, we attribute the recorded features to the enhanced crystallinity of the ternary blend.

The crystalline properties and molecular orientations of PM6: DIBP3F-Se binary and PM6:DIBP3F-Se:BTP-J17 ternary films were also investigated by GIWAXS (Figs. 3g-3j and Table S9). The PM6:DIBP3F-Se binary blend shows a prominent face-on orientation, featuring a (100) laminar diffraction peak located at  $q_{xy}\!\!=0.299\,\mbox{\normalfont\AA}^{-1}$  in the IP direction and  $\pi$ - $\pi$  stacking at  $q_z = 1.675 \text{ Å}^{-1}$  in the OOP direction. The  $d_{(100)}$ ,  $d_{(010)}$ , CCL<sub>(100)</sub>, and CCL<sub>(010)</sub> were then calculated, yielding 21.01, 3.75, 116.35, and 28.87 Å, respectively. In the ternary blend, both  $\pi$ - $\pi$ stacking and lamellar stacking are notably enhanced in the presence of BTP-J17, with  $d_{(100)}$ ,  $d_{(010)}$ ,  $CCL_{(100)}$ ,  $CCL_{(010)}$  becoming 20.87, 3.73, 128.22 and 29.91 Å, respectively. Interestingly, the peak at  $\sim$ 0.39 Å $^{-1}$ in the IP direction, corresponding to DIBP3F-Se:BTP-J17, is preserved in the GIWAXS patterns of the ternary films, suggesting the presence of microdomains associated with the two acceptor materials [47]. The latter feature could partly affect charge transport in ternary-based blends and their devices. These changes indeed suggest that BTP-J17 promotes better molecular packing within the ternary blend, ultimately contributing to the higher  $J_{\rm sc}$  and FF obtained in optimized cells based on the ternary PM6:DIBP3F-Se:BTP-J17 blend.

To investigate the possible impact of BTP-J17 on the vertical distribution of DIBP3F-Se, we utilized time-of-flight secondary ion mass spectrometry (TOF-SIMS) to detect the unique Se in DIBP3F-Se, as depicted in Fig. 4a. The presence of In characteristic of the indium tin oxide (ITO) substrate, indicates proximity to the bottom ITO electrode (see Fig. 2a). Notably, the PM6:DIBP3F-Se binary film shows an

increasing intensity of Se<sup>-</sup> with increasing sputtering time, indicating an increasing concentration of DIBP3F-Se closer to the ITO, whereas the intensity of the Se<sup>-</sup> in the ternary PM6:DIBP3F-Se:BTP-J17 blend remains relatively constant across the BHJ suggesting a more homogeneous distribution. These are important direct observations that highlight the drastic impact of BTP-J17 on the vertical separation of DIBP3F-Se.

To further confirm the differences in the vertical phase separation profile of DIBP3F-Se across the BHJs, depth profile X-ray photoelectron spectroscopy (DP-XPS) measurements were carried out to detect the distinct atomic concentration. Fig. 4b shows that DIBP3F-Se is predominantly located at the bottom of the binary film (arguably on the wrong side of the device), whereas its distribution is notably more uniform in the ternary film, consistent with the TOF-SIMS results. It is important to note that the increasing trend of Se<sup>-</sup> in the binary film aligns well with the requirements of the inverted device architecture (Figure S19 and Table S10). The incorporation of BTP-J17 results in a more homogeneous vertical distribution of DIBP3F-Se, aligning closely with the ideal distribution for acceptor materials. We believe this uniform distribution helps the charge extraction by minimizing material aggregation, reducing bimolecular recombination, facilitating the transport of holes and electrons toward their respective electrodes, and thereby enhancing the overall cell performance.

To elucidate the origin of the higher  $V_{\rm oc}$  observed in the ternary BHJ, the voltage losses ( $V_{\rm loss}$ ) in both binary and ternary OPVs were analyzed using sensitive external quantum efficiency (sEQE) and electroluminescence (EL) measurements (Figs. 4c-4e). The total energy loss,  $E_{\rm loss}$ , and the three main energy loss mechanisms, namely, radiative losses

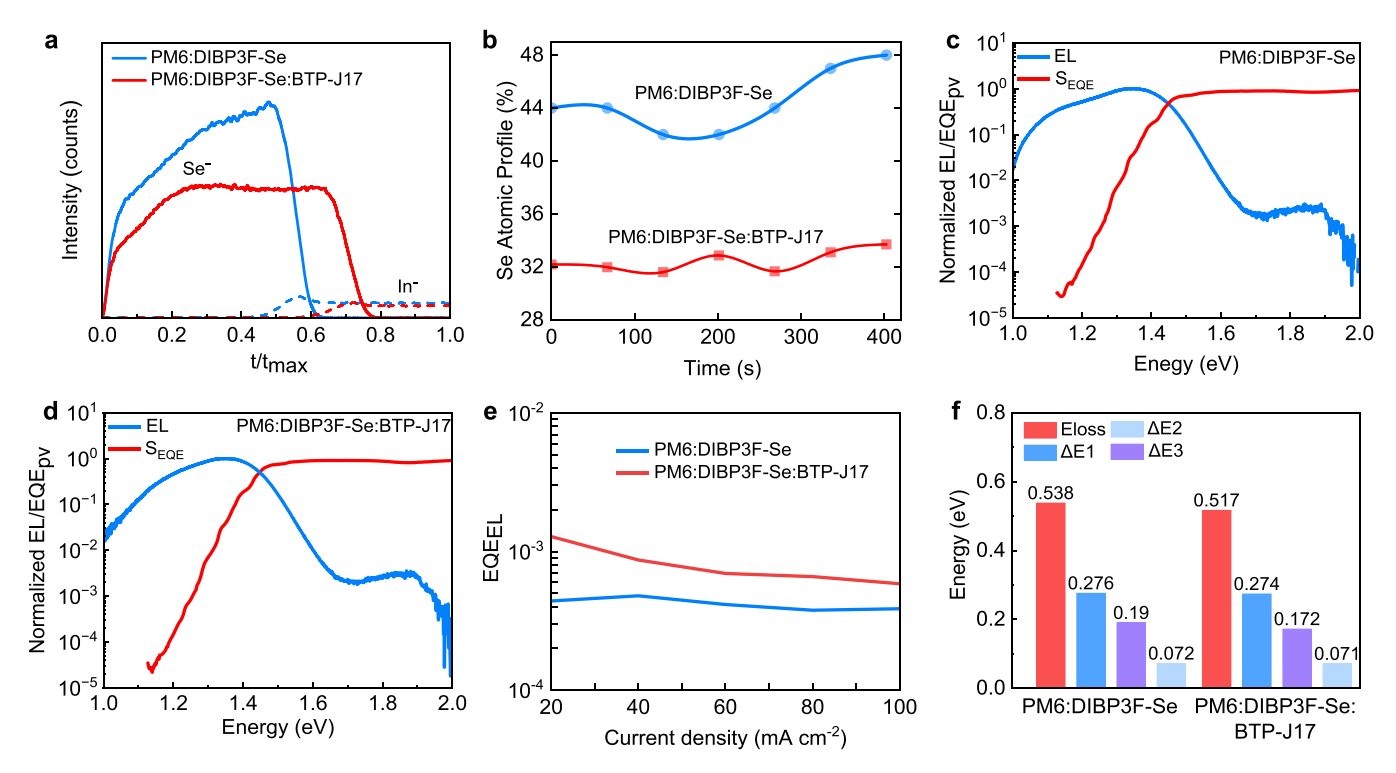


Fig. 4. Blend and device physics characterization. (a) TOF-SIMS for the BHJ films. (b) Depth-Profile XPS for the BHJ films. (c) The sEQE and EL spectra of PM6: DIBP3F-Se OPV. (d) The sEQE and EL spectra of PM6:DIBP3F-Se: BTP-J17 OPV. (e) EL quantum efficiencies of PM6:DIBP3F-Se based binary and PM6:DIBP3F-Se: BTP-J17 based ternary OPVs. (f) Schematic diagram for energy losses of the two types of OPVs.

above the band gap ( $\Delta E_1$ ), radiative recombination energy losses ( $\Delta E_2$ ), and non-radiative recombination energy losses ( $\Delta E_3$ ), were analysed [48,49]. The equations and methodology used to calculate the energy losses can be found in the Supplementary Information section. Firstly, the overall E<sub>loss</sub> for the binary and ternary devices were determined to be 0.538 and 0.517 eV, respectively. The calculated energy losses for the two SMA systems are presented in Fig. 4f and Table S11. For both devices, the calculated  $\Delta E_1$  yields comparable values of  $\approx 0.27$  eV. Similarly, the calculated  $\Delta E_2$  values were 0.072 and 0.071 eV for the binary and ternary BHJ cells, respectively. Finally, the  $\Delta E_3$  for both cells remains remarkably low; 0.190 eV for the binary and 0.172 eV for the ternary BHJ. These values are in broad agreement with those derived from the electroluminescence external quantum efficiency (EQE<sub>EL</sub>) measurements, where:  $q\Delta V_{non-rad} = -kT ln(EQE_{EL})$  [50]. A higher EQE<sub>EL</sub> on the order of  $\approx 8 \times 10^{-4}$  was measured in the PM6:DIBP3F-Se: BTP-J17 ternary device, compared to that of the PM6:DIBP3F-Se ( $\approx$ 4 ×10<sup>-4</sup>) based one, leading to a lower  $\Delta V_{non-rad}$  of 0.180 eV for the ternary device, compared to 0.196 eV for the binary device. These results indicate that adding BTP-J17 as the third component in the BHJ reduces non-radiative recombination losses, thus enhancing the VOC. These remarkable findings highlight a promising path for achieving a higher  $V_{\rm OC}$ .

We also employed Density Functional Theory (DFT) calculations [51] to study the interactions between donor and acceptor materials [52]. Based on the DFT results (Figure S20-S24), both DIBP3F-Se and BTP-J17 possess sites with positive electrostatic potential, which could, in principle, make charge separation easier [53]. On the other hand, the molecular dipole moments of DIBP3F-Se and BTP-J17 are significant (4.51 and 6.11 Debye, respectively), and can facilitate the self-assembly of molecules to ordered molecular domains [54,55]. Another important feature revealed by the DFT calculations (as shown in pertinent Figures S23 and S24) is that the interactions between a BTP-J17 and a DIBP3F-Se molecule create distinct complexes wherein, either the former BTP-J17 moiety may serve as a type of an "electronic bridge" between neighboring DIBP3F-Se acceptors, or the DIBP3F-Se molecule

changes its conformation to the more extended S shape. Both possibilities can enhance electron hopping at longer distances and benefit charge transport [28]. This is an important finding that could explain, at least partly, the improvements in charge transport and overall performance in cells based on optimized ternary blend compositions.

Indeed, since the frontier orbitals of the two molecules (in particular, their lowest unoccupied orbitals) have similar energies (Figures S23 and S24) and significant overlaps, it is relatively easy for excited electrons in these states to hop from the DIBP3F-Se $_{\rm LUMO}$  to the BTP-J17 $_{\rm LUMO+1}$  (or BTP-J17 $_{\rm LUMO+2}$ ) and vice versa. With respect to  $V_{\rm oc}$ , the DFT results are consistent with the experimental data in the sense that the LUMO energy of BTP-J17 is higher than that of DIBP3F-Se. Overall, the DFT-inferred points corroborate the beneficial role of the relatively smaller (and thus more mobile) BTP-J17 molecules on the systems of interest.

Finally, we evaluated the outdoor performance of the binary PM6: DIBP3F-Se and ternary PM6:DIBP3F-Se:BTP-J17 cells with the structure of ITO/PEDOT:PSS/Active Layer/PNDIT-F3N/Ag. To ensure prolonged operation under solar irradiance and high tolerance to temperature fluctuations during day-night cycles, the devices were encapsulated using a glass/glass structure, using butyl rubber as edge sealant with thermoplastic polyurethane to prevent water and oxygen diffusion (Fig. 5a) [56]. Outdoor stability tests were conducted in a hot and sunny climate within the King Abdullah University of Science and Technology (KAUST) campus, Thuwal, Kingdom of Saudi Arabia. The solar irradiance levels during testing ranged from 850 to 1200 W/m<sup>2</sup> at noon from April 17 to June 12, 2024 (Fig. 5b), as measured by a calibrated pyrometer. The recorded highest/lowest air temperatures during daytime/nighttime were 45  $^{\circ}\text{C}/22$   $^{\circ}\text{C},$  with the device temperature approximately 15–20 °C higher (Fig. 5c) [57], while the average relative humidity was  $\approx$  58 %. The power generation density (PGD) exhibited an upward trend from sunrise to noon, followed by a downward trend from noon to sunset. For comparative analysis, device performance at noon was normalized to monitor outdoor degradation (Fig. 5d, e). Devices were biased under open-circuit conditions during time gaps, and J-V curves were recorded at 10-minute intervals. The performance of the

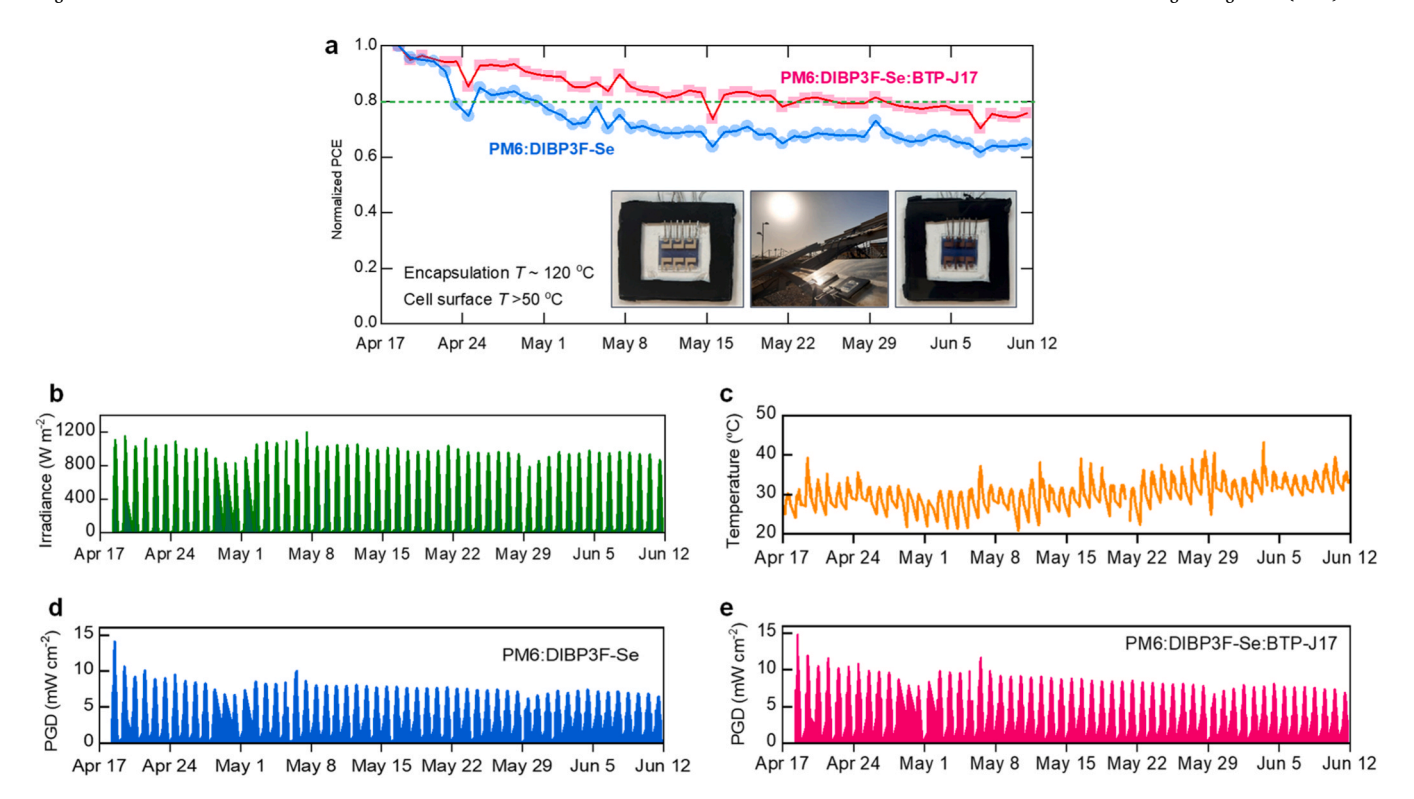


Fig. 5. Stability analysis of binary and ternary BHJ-based OPVs. (a) Normalized PCE for the encapsulated cells measured at noontime every day. Inset: photographs depicting the actual devices used for the testing (left and right) and the outdoor experimental settings (middle). The outdoor stability analysis was carried out within the KAUST campus in Thuwal, Kingdom of Saudi Arabia, from April 18th to June 12th 2024. The average relative humidity during the testing period was  $\approx 63 \%$ . J–V curves were measured every 10 min during the daytime. (b) Solar irradiance measured during the test period. (c) Air temperature measured during the test period. Power generation density (PGD) of the encapsulated (d) PM6:DIBP3F-Se and (e) PM6:DIBP3F-Se:BTP-J17 cells, respectively.

ternary PM6:DIBP3F-Se:BTP-J17 cell as found to degrade less during the first week, an effect most likely attributed to the more thermodynamically stable BHJ [58,59]. Thermal stability measurements of the cells at 85°C were also performed to assess the role of heat-induced degradation on outdoor stability (Figure S25). The higher thermal stability of the ternary BHJ indicates the higher tolerance of morphology-related degradation of the photoactive layer under light and heat stress. It may also be argued that the ability of BTP-J17 to reduce the propensity of DIBP3F-Se to agglomerate (as suggested by the TOF-SIMS data) results in a more stable phase separation and PCE [60,61]. It is worth noting that PM6:DIBP3F-Se:BTP-J17 cells still have ~80 % of the initial performance after 7 weeks of exposure to the rather harsh outdoor environment (e.g. high temperature, long days, high relative humidity) in Saudi Arabia. This preliminary operating stability study provides the groundwork for further research into the effects of solar irradiation and heat-stress on the outdoor stability of state-of-the-art OPVs.

#### 3. Conclusion

In conclusion, we designed and synthesized an asymmetric SMA, named BTP-J17, and used it as the third component in PM6:DIBP3F-Se based OPVs. BTP-J17 exhibits a blue-shifted absorption spectrum compared to DIBP3F-Se, and when the two components are blended the ensuing layers exhibit an enhanced absorption coefficient. Experimental investigations indicated that BTP-J17 diffuses to the PM6/DIBP3F-Se interface, improving exciton separation and enhancing charge carrier transport while stabilizing the morphology of the BHJ. Crucially, the addition of BTP-J17 at optimal concentrations was found to suppress recombination losses, as revealed by exciton kinetics studies. These advantageous characteristics enabled the development of OPVs with a champion PCE of 19.60 %. By incorporating a 100-nm-thick MgF<sub>2</sub> as the antireflection layer and n-doping the ternary PM6:DIBP3F-Se:BTP-J17

BHJ with the molecular dopant ethyl viologen, the cell's maximum PCE (uncertified) was further increased to 20.5 % ( $J_{SC}=27.85~\text{mA}~\text{cm}^{-2}$ ,  $V_{OC}=0.942~\text{V}$ , FF = 78.35 %). Along with their superior performance, the optimized ternary BHJ-based cells showed improved operational stability under outdoor testing in Saudi Arabia, with a  $T_{80}$  time of seven weeks. The present work offers new insights into how an asymmetric SMA can help boost the performance of OPVs, highlighting a promising strategy for enhancing the overall performance of state-of-the-art OPVs.

#### CRediT authorship contribution statement

Stefaan De Wolf: Supervision, Data curation. Xiaoming Chang: Formal analysis, Data curation. Hendrik Faber: Formal analysis, Data curation. Hanlin Hu: Formal analysis. Dipti Naphade: Formal analysis, Data curation. Han Young Woo: Formal analysis. Maxime Babics: Formal analysis, Data curation. Donghong Yu: Supervision. Elefterios Lidorikis: Supervision. Ergang Wang: Writing - review & editing, Supervision, Project administration, Investigation. Mohamad Insan Nugraha: Data curation. Zhaoheng Ling: Writing - original draft, Investigation, Formal analysis, Data curation, Conceptualization. Leonidas Tsetseris: Software, Formal analysis. Frédéric Laquai: Supervision. Spyros Doukas: Formal analysis. Yuanbao Lin: Formal analysis. Christopher E. Petoukhoff: Writing – review & editing, Formal analysis, Data curation. Xiaokang Sun: Formal analysis. Sang Young Jeong: Formal analysis, Data curation. Thomas D. Anthopoulos: Writing - review & editing, Supervision, Project administration, Investigation. Mingjie He: Software. Jingnan Wu: Writing - review & editing, Formal analysis, Data curation. Maryam Alqurashi: Formal analysis. José P. Jurado: Writing - review & editing, Data curation.

#### **Declaration of Competing Interest**

The authors declare that they have no known competing financial interests or personal relationships that could have appeared to influence the work reported in this paper.

#### Acknowledgements

This publication is based upon work supported by the King Abdullah University of Science and Technology (KAUST) Office of Sponsored Research (OSR) under Award Nos. OSR- 2018-CARF/CCF-3079, OSR-2019-CRG8-4095 and ORA-CRG10-2021-4681. This work was also carried out within the framework of the Action 'Flagship Research Projects in challenging interdisciplinary sectors with practical applications in Greek Industry', implemented through the National Recovery and Resilience Plan Greece 2.0 and funded by the European Union -Next Generation EU (project code: TAEDR- 537347), and the Horizon 2020 Framework Programme Project MUSICODE (No 953187). The DFT calculations used the GRNET-ARIS HPC resources under project 15002. H.Y.W. acknowledges the financial support from National Research Foundation of Korea (2019R1A6A1A11044070, RS-2024-00334832). C. E.P. acknowledges support from KAUST Global Fellowship Program under Award No. ORA-2022-5002. E.W. thanks the Swedish Research Council, the Swedish Research Council Formas, STINT (MG2021-9063) and The Knut and Alice Wallenberg Foundation (2022.0192) for financial support. D.H.Y support from Sino-Danish Center (SDC) for Education and Research is fully acknowledged.

#### Appendix A. Supporting information

Supplementary data associated with this article can be found in the online version at doi:10.1016/j.mser.2024.100922.

#### Data availability

Data will be made available on request.

#### References

- [1] X. Yu, P. Ding, D. Yang, P. Yan, H. Wang, S. Yang, J. Wu, Z. Wang, H. Sun, Z. Chen, L. Xie, Z. Ge, Angew. Chem. Int. Ed. (2024) e202401518.
- [2] K. Liu, Y. Jiang, G. Ran, F. Liu, W. Zhang and X. Zhu, Joule, (doi:10.1016/J.JOULE. 2024.01.005).
- [3] J. Song, C. Zhang, C. Li, J. Qiao, J. Yu, J. Gao, X. Wang, X. Hao, Z. Tang, G. Lu, R. Yang, H. Yan, Y. Sun, Angew. Chem. Int. Ed. (2024) e202404297.
- [4] Y. Zhang, W. Deng, C.E. Petoukhoff, X. Xia, Y. Lang, H. Xia, H. Tang, H.T. Chandran, S. Mahadevan, K. Liu, P.W.K. Fong, Y. Luo, J. Wu, S.-W. Tsang, F. Laquai, H. Wu, X. Lu, Y. Yang and G. Li, *Joule*, (doi:10.1016/J.JOULE.2023.12.009).
- [5] S. Guan, Y. Li, C. Xu, N. Yin, C. Xu, C. Wang, M. Wang, Y. Xu, Q. Chen, D. Wang, L. Zuo, H. Chen, Adv. Mater. (2024) 2400342.
- [6] H. Chen, S.Y. Jeong, J. Tian, Y. Zhang, D.R. Naphade, M. Alsufyani, W. Zhang, S. Griggs, H. Hu, S. Barlow, H.Y. Woo, S.R. Marder, T.D. Anthopoulos, I. McCulloch, Y. Lin, Energy Environ. Sci. 16 (2023) 1062–1070.
- [7] Y. Xie, C. Zhou, X. Ma, S.Y. Jeong, H.Y. Woo, F. Huang, Y. Yang, H. Yu, J. Li, F. Zhang, K. Wang, X. Zhu, Y. Xie, C. Zhou, X. Ma, F. Huang, Y. Yang, H. Yu, J. Li, F. Zhang, K. Wang, X. Zhu, S.Y. Jeong, H.Y. Woo, Adv. Energy Mater. (2024) 2400013.
- [8] S.N. Afraj, B.H. Jiang, Y.W. Su, C.H. Yang, H.S. Shih, A. Velusamy, J.S. Ni, Y. Ezhumalai, T.Y. Su, C.L. Liu, S. Yau, C.P. Chen, M.C. Chen, J. Mater. Chem. C. 12 (2024) 2247–2257.
- [9] C.Y. Lin, B.H. Jiang, P.J. Weng, Y. Hsuan Lin, Y.W. Su, H.S. Shih, Z.E. Shi, Y.R. Lin, J. Vailassery, S.S. Sun, C.P. Chen, Y.J. Chang, Chem. Eng. J. 494 (2024) 153183.
- [10] W. Wei, X. Zhou, S. Pang, J. Zhou, X. Yuan, J. Li, Y. Chen, L. Pan, Z. Xie, H. Wu, F. Huang, Y. Cao, C. Duan, Aggregate (2024), e488.
- F. Huang, Y. Cao, C. Duan, Aggregate (2024) e488.
  [11] W. Su, X. Zhou, Z.-F. Yao, H. Bai, Y. Duan, R. Sun, Y. Wu, Q. Wu, H. Qin, C. Zhao, W. Zhu, H.Y. Woo, J. Min, Y. Li, W. Ma, Q. Fan, W. Su, X. Zhou, H. Qin, Y. Li, H. Bai, Q. Wu, C. Zhao, W. Ma, Q. Fan, W. Zhu, Adv. Funct. Mater. (2024) 2313744.
- [12] S. Mahadevan, T. Liu, S.M. Pratik, Y. Li, H.Y. Ho, S. Ouyang, X. Lu, H.-L. Yip, P.C. Y. Chow, J.-L. Brédas, V. Coropceanu, S.K. So, S.-W. Tsang, Nat. Commun. 2024 151 15 (2024) 1–10.
- [13] S. Chen, S. Zhu, L. Hong, W. Deng, Y. Zhang, Y. Fu, Z. Zhong, M. Dong, C. Liu, X. Lu, K. Zhang, F. Huang, Angew. Chem. Int. Ed. (2024) e202318756.

- [14] C. Xie, X. Zeng, C. Li, X. Sun, S. Liang, H. Huang, B. Deng, X. Wen, G. Zhang, P. You, C. Yang, Y. Han, S. Li, G. Lu, H. Hu, N. Li and Y. Chen, *Energy Environ. Sci.*, (doi:10.1039/D4EE00068D).
- [15] N. Zhang, K. Jiang, F.R. Lin, Y. An, G. Du, T. Xia, A.K.-Y. Jen, H.-L. Yip, Mater. Today Energy (2024) 101548.
- [16] H. Hu, S. Liu, J. Xu, R. Ma, Z. Peng, T. Archie, D. Peña, Y. Cui, W. Liang, X. Zhou, S. Luo, H. Yu, M. Li, J. Wu, S. Chen, G. Li, Y. Chen, Angew. Chem. Int. Ed. (2024) e202400086.
- [17] R. Xu, Y. Jiang, F. Liu, G. Ran, K. Liu, W. Zhang, X. Zhu, R. Xu, Y. Jiang, F. Liu, K. Liu, X. Zhu, G. Ran, W. Zhang, Adv. Mater. (2024) 2312101.
- [18] J.W. Lee, C. Sun, J. Lee, D.J. Kim, W.J. Kang, S. Lee, D. Kim, J. Park, T.N.L. Phan, Z. Tan, F.S. Kim, J.Y. Lee, X. Bao, T.S. Kim, Y.H. Kim, B.J. Kim, Adv. Energy Mater. 14 (2024) 2303872.
- [19] M. Dong, S. Chen, L. Hong, J. Jing, Y. Bai, Y. Liang, C. Zhu, T. Shi, W. Zhong, L. Ying, K. Zhang, F. Huang, Nano Energy 119 (2024) 109097.
- [20] J.-W. Lee, G.-U. Kim, D.J. Kim, Y. Jeon, S. Li, T.-S. Kim, J.-Y. Lee, B.J. Kim, J.-W. Lee, G.-U. Kim, S. Li, B.J. Kim, D.J. Kim, T.-S. Kim, Y. Jeon, J.-Y. Lee, Adv. Energy Mater. 12 (2022) 2200887.
- [21] Y. Qin, N. Balar, Z. Peng, S. Kashani, J. Hou, H. Ade, Joule 5 (2021) 2129-2147.
- [22] Q. Fan, W. Su, S. Chen, H. Yan, D. Yu, E. Wang, W. Kim, X. Chen, B. Lee, T. Liu, U. A. Mé Ndez-Romero, R. Ma, T. Yang, W. Zhuang, Y. Li, Y. Li, T.-S. Kim, L. Hou and C. Yang, (doi:10.1016/j.joule.2020.01.014).
- [23] H. Jeon, K.P. Hong, J.W. Lee, D. Jeong, T.N.L. Phan, H.G. Lee, J.S. Park, C. Wang, S. Xuyao, Y.H. Kim, B.J. Kim, Chem. Mater. 35 (2023) 9276–9286.
- [24] C. Sun, J.W. Lee, C. Lee, D. Lee, S. Cho, S.K. Kwon, B.J. Kim, Y.H. Kim, Joule 7 (2023) 416–430.
- [25] M. Lv, Q. Wang, J. Zhang, Y. Wang, Z.G. Zhang, T. Wang, H. Zhang, K. Lu, Z. Wei, D. Deng, Adv. Mater. 36 (2024) 2310046.
- [26] Y. Liang, D. Zhang, Z. Wu, T. Jia, L. Lüer, H. Tang, L. Hong, J. Zhang, K. Zhang, C. J. Brabec, N. Li, F. Huang, Nat. Energy 2022 712 7 (2022) 1180–1190.
- [27] H. Wang, C. Cao, H. Chen, H. Lai, C. Ke, Y. Zhu, H. Li, F. He, Angew. Chem. 134 (2022) e202201844.
- [28] J. Wu, Z. Ling, L.R. Franco, S.Y. Jeong, Z. Genene, J. Mena, S. Chen, C. Chen, C. M. Araujo, C.F.N. Marchiori, J. Kimpel, X. Chang, F.H. Isikgor, Q. Chen, H. Faber, Y. Han, F. Laquai, M. Zhang, H.Y. Woo, D. Yu, T.D. Anthopoulos, E. Wang, Angew. Chem. Int. Ed. 62 (2023) e202302888.
- [29] L. Zhan, S. Li, Y. Li, R. Sun, J. Min, Y. Chen, J. Fang, C.Q. Ma, G. Zhou, H. Zhu, L. Zuo, H. Qiu, S. Yin, H. Chen, Adv. Energy Mater. 12 (2022) 2201076.
- [30] T. Chen, S. Li, Y. Li, Z. Chen, H. Wu, Y. Lin, Y. Gao, M. Wang, G. Ding, J. Min, Z. Ma, H. Zhu, L. Zuo, H. Chen, T. Chen, S. Li, Y. Li, H. Wu, M. Wang, G. Ding, L. Zuo, H. Chen, H. Zhu, Z. Chen, Y. Gao, J. Min, Adv. Mater. (2023) 2300400.
- [31] J. Huang, T. Chen, L. Mei, M. Wang, Y. Zhu, J. Cui, Y. Ouyang, Y. Pan, Z. Bi, W. Ma, Z. Ma, H. Zhu, C. Zhang, X.-K. Chen, H. Chen, L. Zuo, Nat. Commun. 2024 151 15 (2024) 1–11.
- [32] F.D. Eisner, M. Azzouzi, Z. Fei, X. Hou, T.D. Anthopoulos, T.J.S. Dennis, M. Heeney, J. Nelson, J. Am. Chem. Soc. 141 (2019) 6362–6374.
- [33] J. Rivnay, S.C.B. Mannsfeld, C.E. Miller, A. Salleo, M.F. Toney, Chem. Rev. 112 (2012) 5488–5519.
- [34] Y. Cai, Y. Li, R. Wang, H. Wu, Z. Chen, J. Zhang, Z. Ma, X. Hao, Y. Zhao, C. Zhang, F. Huang, Y. Sun, Adv. Mater. 33 (2021) 2101733.
- [35] H. Xia, Y. Zhang, K. Liu, W. Deng, M. Zhu, H. Tan, P.W.K. Fong, H. Liu, X. Xia, M. Zhang, T.A. Dela Peña, R. Ma, M. Li, J. Wu, Y. Lang, J. Fu, W.-Y.Y. Wong, X. Lu, W. Zhu, G. Li, Energy Environ. Sci. 16 (2023) 6078–6093.
- [36] S. Wu, J. Polym. Sci. Part C. Polym. Symp. 34 (1971) 19–30.
- [37] M. Sumita, K. Sakata, S. Asai, K. Miyasaka, H. Nakagawa, Polym. Bull. 25 (1991) 265–271.
- [38] H. Bin, K. Datta, J. Wang, T.P.A. Van Der Pol, J. Li, M.M. Wienk, R.A.J. Janssen, ACS Appl. Mater. Interfaces 14 (2022) 16497–16504.
- [39] Z. Ling, M.I. Nugraha, W.T. Hadmojo, Y. Lin, S.Y. Jeong, E. Yengel, H. Faber, H. Tang, F. Laquai, A.H. Emwas, X. Chang, T. Maksudov, M. Gedda, H.Y. Woo, I. McCulloch, M. Heeney, L. Tsetseris, T.D. Anthopoulos, ACS Energy Lett. 8 (2023) 4104–4112.
- [40] J.I. Khan, R.S. Ashraf, M.A. Alamoudi, M.N. Nabi, H.N. Mohammed, A. Wadsworth, Y. Firdaus, W. Zhang, T.D. Anthopoulos, I. McCulloch, F. Laquai, Sol. RRL 3 (2019) 1900023
- [41] J.I. Khan, M.A. Alamoudi, N. Chaturvedi, R.S. Ashraf, M.N. Nabi, A. Markina, W. Liu, T.A. Dela Peña, W. Zhang, O. Alévêque, G.T. Harrison, W. Alsufyani, E. Levillain, S. De Wolf, D. Andrienko, I. McCulloch, F. Laquai, Adv. Energy Mater. 11 (2021) 2100839.
- [42] S. Karuthedath, J. Gorenflot, Y. Firdaus, N. Chaturvedi, C.S.P. De Castro, G. T. Harrison, J.I. Khan, A. Markina, A.H. Balawi, T.A. Dela Peña, W. Liu, R.Z. Liang, A. Sharma, S.H.K. Paleti, W. Zhang, Y. Lin, E. Alarousu, D.H. Anjum, P. M. Beaujuge, S. De Wolf, I. McCulloch, T.D. Anthopoulos, D. Baran, D. Andrienko, F. Laquai, Nat. Mater. 2020 203 20 (2020) 378–384.
- [43] N.A. Ran, J.A. Love, M.C. Heiber, X. Jiao, M.P. Hughes, A. Karki, M. Wang, V. V. Brus, H. Wang, D. Neher, H. Ade, G.C. Bazan, T.Q. Nguyen, Adv. Energy Mater. 8 (2018) 1701073.
- [44] J. Wu, J. Lee, Y.C. Chin, H. Yao, H. Cha, J. Luke, J. Hou, J.S. Kim, J.R. Durrant, Energy Environ. Sci. 13 (2020) 2422–2430.
- [45] E.P. Yao, C.C. Chen, J. Gao, Y. Liu, Q. Chen, M. Cai, W.C. Hsu, Z. Hong, G. Li, Y. Yang, Sol. Energy Mater. Sol. Cells 130 (2014) 20–26.
- [46] X. Wang, J. Wang, P. Wang, C. Han, F. Bi, J. Wang, N. Zheng, C. Sun, Y. Li, X. Bao, Adv. Mater. 35 (2023) 2305652.
- [47] C. Yang, Q. An, M. Jiang, X. Ma, A. Mahmood, H. Zhang, X. Zhao, H.F. Zhi, M. H. Jee, H.Y. Woo, X. Liao, D. Deng, Z. Wei, J.L. Wang, Angew. Chem. Int. Ed. 62 (2023) e202313016.

- [48] Y. Guo, Z. Chen, J. Ge, J. Zhu, J. Zhang, Y. Meng, Q. Ye, S. Wang, F. Chen, W. Ma, Z. Ge, Adv. Funct. Mater. 33 (2023) 2305611.
- [49] W. Peng, Y. Lin, S.Y. Jeong, Z. Genene, A. Magomedov, H.Y. Woo, C. Chen, W. Wahyudi, Q. Tao, J. Deng, Y. Han, V. Getautis, W. Zhu, T.D. Anthopoulos, E. Wang, Nano Energy 92 (2022) 106681.
- [50] U. Rau, Phys. Rev. B Condens. Matter Mater. Phys. 76 (2007) 085303.
- [51] N. Godbout, D.R. Salahub', J. Andzelm' and E. Wimmer, https://doi.org/10.113 9/v92-079, 2011, 70, 560-571.
- [52] K. Momma and F. Izumi, urn:issn:0021-8898, 2011, 44, 1272-1276.
- [53] H. Yao, Y. Cui, D. Qian, C.S. Ponseca, A. Honarfar, Y. Xu, J. Xin, Z. Chen, L. Hong, B. Gao, R. Yu, Y. Zu, W. Ma, P. Chabera, T. Pullerits, A. Yartsev, F. Gao, J. Hou, J. Am. Chem. Soc. 141 (2019) 7743–7750.
- [54] C. Li, H. Fu, T. Xia, Y. Sun, Adv. Energy Mater. 9 (2019) 1900999.
- [55] W. Gao, M. Zhang, T. Liu, R. Ming, Q. An, K. Wu, D. Xie, Z. Luo, C. Zhong, F. Liu, F. Zhang, H. Yan, C. Yang, Adv. Mater. 30 (2018) 1800052.
- [56] X. Du, T. Heumueller, W. Gruber, A. Classen, T. Unruh, N. Li, C.J. Brabec, Joule 3 (2019) 215–226.
- [57] E. Aydin, T.G. Allen, M. De Bastiani, L. Xu, J. Ávila, M. Salvador, E. Van Kerschaver, S. De Wolf, Nat. Energy 2020 511 5 (2020) 851–859.
- [58] L. Ye, B.A. Collins, X. Jiao, J. Zhao, H. Yan, H. Ade, Adv. Energy Mater. 8 (2018) 1703058.
- [59] Y. Liu, M. Li, X. Zhou, Q.Q. Jia, S. Feng, P. Jiang, X. Xu, W. Ma, H.B. Li, Z. Bo, ACS Energy Lett. 3 (2018) 1832–1839.
- [60] Y. Liang, D. Zhang, Z. Wu, T. Jia, L. Lüer, H. Tang, L. Hong, J. Zhang, K. Zhang, C. J. Brabec, N. Li, F. Huang, Nat. Energy 2022 712 7 (2022) 1180–1190.
- [61] R. Sun, W. Wang, H. Yu, Z. Chen, X.X. Xia, H. Shen, J. Guo, M. Shi, Y. Zheng, Y. Wu, W. Yang, T. Wang, Q. Wu, Y. (Michael) Yang, X. Lu, J. Xia, C.J. Brabec, H. Yan, Y. Li, J. Min, Joule 5 (2021) 1548–1565.



Zhaoheng Ling received the B.S. degree in power materials science and engineering from Hefei University, Hefei, China, in 2013. He is involved in a joint master program between the University of Science and Technology of China, Suzhou, China, and the Ningbo Institute of Materials Technology and Engineering, Chinese Academy of Sciences, Ningbo, China. Then he works in KU Leuven/IMEC for 2.5 years. After this, he joined Prof. Thomas D. Anthopoulos group in KAUST for Ph. D study. His current research interest is device physics of organic solar cells.



Thomas D. Anthopoulos is a Professor of Emerging Optoelectronics at the University of Manchester in the UK. Following the award of his B.Eng. and D.Phil. degrees, he spent two years at the University of St. Andrews (UK), where he worked on organic semiconductors for light-emitting diodes before joining Philips Research Laboratories in The Netherlands to focus on printable microelectronics. From 2006–2017, he held faculty positions at Imperial College London (UK), first as an EPSRC Advanced Fellow and later as a Reader and Professor of Experimental Physics. From 2017–2023, he was a Professor of Material Science at King Abdullah University of Science and Technology (KAUST) in Saudi Arabia. His research interests are diverse and cover the development and application of novel processing

paradigms and the physics, chemistry, and application of functional materials.